LIMNOLOGY
and
OCEANOGRAPHY: METHODS

ASLO

Limnol. Oceanogr.: Methods 23, 2025, 624–637

doi: 10.1002/lom3.10709

NEW METHODS

Embedding a multichannel ion-sensitive field-effect transistor-pH sensor array in marine sediments: a new approach for continuous in situ pH monitoring

Yoshita Ogawa,[1,2] Shoji Yamamoto ,[1]*+ Kenta Suzuki,[1] Kazuhiro Morioka,[3] Akihide Hemmi,[4] Hajime Kayanne,[5] Hizuru Nakajima[1]

[1]Department of Applied Chemistry, Graduate School of Urban Environmental Sciences, Tokyo Metropolitan University, Tokyo, Japan; [2]Hioki E.E. Corporation, Nagano, Japan; [3]Department of Biomedical Analysis, School of Pharmacy, Tokyo University of Pharmacy and Life Sciences, Tokyo, Japan; [4]Mebius Advanced Technology Ltd, Tokyo, Japan; [5]Department of Earth and Planetary Science, The University of Tokyo, Tokyo, Japan

Abstract

Human activities have significantly increased carbon dioxide emissions, leading to global warming and ocean acidification, which threaten marine ecosystems, including coral reefs with high biodiversity. Coral reef maintenance relies on a balance between calcium carbonate formation and dissolution. Among the processes, sandy sediments, covering vast areas and highly sensitive to ocean acidification, require urgent investigations to elucidate their dissolution mechanisms. However, conventional glass electrodes have limitations in continuous monitoring of the spatiotemporal distribution of pH within sediment. To address this, we developed a multichannel ion-sensitive field-effect transistor (ISFET)-pH sensor array with a tantalum oxide sensing membrane, which was embedded in the sediment to enable high-resolution and continuous pH monitoring. A 24-h pH monitoring experiment was conducted in coral reef sediments to validate the method. The performance of the sensor was evaluated through both laboratory and field observations, and a comparison with a conventional glass electrode confirmed that the ISFET-pH sensor provided stable pH measurements within the uncertainty range of the glass electrode. The developed sensor array is a low-cost and durable automatic measurement system, offering an alternative to conventional glass electrodes, which are expensive and fragile. However, optimizing sputtering conditions, annealing processes, and data processing techniques is necessary to reduce environmental influences and enhance measurement accuracy. The proposed array-based observation method enables the acquisition of high-resolution vertical pH profiles and is expected to contribute to the quantitative evaluation of the chemical role of sandy sediments and the elucidation of carbon cycling in coral reef ecosystems.

Increased carbon dioxide (CO_2) emissions from human activities have catalyzed global warming and accelerated ocean acidification. Observations since the Industrial Revolution indicate a decline in the average pH of surface seawater by 0.1 pH, with projections estimating a further decrease of 0.3–0.4 pH by the end of this century (Orr et al. 2005; Doney et al. 2009). Ocean acidification impairs skeletal formation in marine organisms with calcium carbonate ($CaCO_3$) shells, such as corals and mollusks, and facilitates the dissolution of sandy sediments within coral reefs, threatening these vital ecosystems (Andersson et al. 2009; Kroeker et al. 2013; Tribollet et al. 2009). Coral reefs are self-perpetuating

*Correspondence: shoji-yamamoto@tmu.ac.jp

Associate editor: Hayley Schiebel

+Yoshita Ogawa and Shoji Yamamoto contributed equally to this work.

Data Availability Statement: The datasets generated and analyzed in this study were deposited in the Zenodo repository and are available at https://doi.org/10.5281/zenodo.15123056.

ecosystems where $CaCO_3$ formation and accretion are essential for structural complexity and biodiversity. The overall growth or decline of coral reef ecosystems is determined by the balance between $CaCO_3$ production (calcification) and its loss owing to dissolution and physical damage from events such as storms (Eyre et al. 2014). The $CaCO_3$ reserves within coral reefs are distributed mainly between coral skeletons and sediments, with sediments often occupying the largest geomorphological zones in numerous ecosystems. For example, sediments cover 95% of the surface area of the southwestern New Caledonia reef complex (Gattuso et al. 1998). Ocean acidification suppresses calcification and enhances $CaCO_3$ dissolution, both of which contribute to the decline of coral reef ecosystems. Recent studies indicate that the impact of ocean acidification on $CaCO_3$ dissolution is more notable than its effect on calcification (Andersson et al. 2013; Eyre et al. 2018), potentially shifting coral reef ecosystems from net accretion to net erosion. However, the specifics of when, at what rate, and under which seawater temperatures and CO_2 concentrations the shift occurs remain unclear (Andersson et al. 2009; Dove et al. 2013; Silverman et al. 2009).

To address the challenges above, the mechanisms of $CaCO_3$ dissolution within sediments must be investigated. Pore water pH plays a crucial role in determining the dissolution rate of reactive mineral layers, such as $CaCO_3$, and influences microbial metabolic activity within sediments (Soetaert et al. 2007; Yanagawa et al. 2013). Conversely, $CaCO_3$ dissolution and organism and bacterial activity can alter the surrounding pH, establishing a dynamic feedback loop (Widdicombe et al. 2009; Yamamoto et al. 2015). The feedback mechanism can either enhance or buffer changes in carbonate chemistry, depending on environmental conditions such as temperature, total alkalinity, and organic matter decomposition. Therefore, the spatiotemporal pH distributions within sediments are essential indicators of the long-term biogeochemical reactivity and carbon-buffering capacity of marine systems (Shao et al. 2023).

Traditional methods of measuring pore water pH in marine sediments have several limitations. Typically, skilled divers use glass electrodes to assess the vertical pH distribution in marine sediments. This process involves divers descending to the ocean floor and positioning needle-type pH sensors within the sediments, and then moving them vertically at fixed intervals to record pH. However, the application of this method is limited, as glass pH sensors are fragile and expensive, and the process is labor-intensive and physically demanding. Additionally, the electrodes are manually inserted into sediments at millimeter intervals; therefore, recording a single vertical profile takes over 30 min, hindering simultaneous pH distribution measurements. Long-term continuous data collection over several days is unattainable, and adjusting the electrode depth can disrupt sediment conditions, thus precluding continuous true vertical pH measurement.

Ion-sensitive field-effect transistor (ISFET) sensors, which respond selectively to specific ions in solution, have garnered significant attention. ISFET technology, proposed in 1970 by Bergveld (Bergveld 1970), comprises an ion-sensitive membrane attached to the gate electrode that selectively responds to specific ions. These sensors offer several advantages over traditional glass electrodes: they are smaller, more robust, have a rapid response time, and are less expensive (Bergveld 2003). Owing to such features, ISFET technology is suitable for outdoor use with multiple sensors. Common pH-sensitive membranes used in these sensors include silicon dioxide (SiO_2), aluminum oxide (Al_2O_3), and tantalum oxide (Ta_2O_5), selected for their chemical stability and pH sensitivity (Sinha and Pal 2022). An established example is the Durafet sensor by Honeywell (Johnson et al. 2016; Gonski et al. 2018; Martz et al. 2010), which is recognized widely for its high precision and reliable response membrane, typically composed of tantalum oxide. In marine environments, ISFET-based pH sensors typically achieve a precision of ± 0.01 to ± 0.02 pH (Bresnahan et al. 2014; Gonski et al. 2018, 2024; McLaughlin et al. 2017; Miller et al. 2018), making them suitable for weather-quality (± 0.02 pH) but not yet for climate-quality (± 0.003 pH) data, as defined by the Global Ocean Acidification Observing Network (Newton et al. 2015). This level of precision is sufficient for detecting pH variations in sediment porewater that influence $CaCO_3$ dissolution processes, although further refinements are required for applications requiring higher precision, such as spectrophotometric methods (Müller and Rehder 2018). Despite their widespread industrial application, these commercial sensors often lack the customization ability required for specific research applications, such as sediment observations, thus posing a significant challenge in the observation of specific environments or situations (Jimenez-Jorquera et al. 2010).

In the present study, a multichannel ISFET-pH sensor array was developed to overcome the limitations of traditional pH measurement methods for marine sediments. The sensor array uses a response membrane made of tantalum oxide, known for its chemical stability and high pH sensitivity, enabling precise and reliable pH measurements in both the water column and sediment. Considering existing methods for measuring pH in sandy sediments rely primarily on fragile and labor-intensive glass needle electrodes, we compared the performance of our ISFET sensor array against glass electrodes. For standard buffer measurements, pH was determined using the National Bureau of Standards (NBS) scale. In contrast, all pH values measured in tris(hydroxymethyl)aminomethane (Tris) and 2-amino-2-methyl-1-propanol (AMP), as well as in natural seawater, were reported on the total scale to maintain consistency in environmental data interpretation. We evaluated the performance of the sensors through laboratory experiments and field observations, demonstrating their potential for application in continuous pH monitoring in marine sediment environments. This innovative approach could potentially

enhance the monitoring of coral reef ecosystems and broaden our understanding of biogeochemical processes in marine systems.

Materials and procedures

Reagents and materials

Distilled water was purified using a Direct-Q system (Merck Millipore, Tokyo, Japan) and used to clean the ISFET-pH sensor. The pH standard solutions for evaluating sensor performance were sourced from Fuji Film Wako Pure Chemical Corp. (Osaka, Japan) and included borate (pH 9.18), neutral phosphate (pH 6.86), and phthalate (pH 4.01) standard solutions. These buffers are Japan Calibration Service System (JCSS)-certified and traceable to the national metrology standard of Japan. Tris and 2-amino-2-methyl-1-propanol (AMP) (both obtained from Fuji Film Wako Pure Chemical) buffers in artificial seawater used for sensor calibration were prepared according to the standard procedure outlined in SOP 6a (Dickson et al. 2007). The pH of standard buffer solutions (borate, phosphate, and phthalate) was determined using the NBS scale, while the pH values of Tris and AMP buffers, as well as natural seawater, were reported on the total scale to ensure consistency in environmental data interpretation. The natural seawater used in the experiments was collected from the coast of Sesoko Island, Okinawa.

Fabricating the ion-sensitive Ta_2O_5 membrane

Tantalum oxide, serving as the ion-sensitive membrane, was deposited on a 5 × 5-mm silicon wafer using an electron cyclotron resonance sputtering system (Elionix, EIS-200ER) at Tokyo Metropolitan University (Hino campus). The film thickness was optimized at 32 nm with a deposition time of 8 min. The system ionizes argon gas introduced into the chamber by applying an acceleration voltage, thereby generating plasma. This plasma is directed toward the target material, causing the target particles to adhere to the sample and form a thin film. The deposition conditions included an argon gas flow rate of 0.74 standard cm^3/min, accelerating voltage of 2000 V, microwave power of 100 W, and ion emission of 3.0–3.5 mA. The film thickness was measured using a nanoscale hybrid atomic force microscope (AFM; Keyence, VN-8000). The Ta and O photoelectron spectra of the deposited tantalum oxide films were measured using x-ray photoelectron spectroscopy (XPS; JEOL, JPS-9010MX). Surface elemental ratios were calculated based on the ratios of the areas of the spectra. Furthermore, among the observed peaks, those derived from O 1s were isolated and deconvoluted into peaks originating from oxo (═O) and hydroxyl (—OH) groups. By summing the area ratios of these peaks, the ratio of oxo and hydroxyl groups on the tantalum oxide surface was determined, enabling assessment of the film surface composition.

Fabricating the multichannel ISFET-pH sensor array

Following the procedure described in the previous section, ISFET-pH sensors were fabricated using silicon wafers coated with tantalum oxide and field-effect transistors (FETs) (Toshiba Electronic Devices & Storage, 2SK208-Y). Figure 1 illustrates the fabrication process of the ISFET-pH sensor. Initially, the non-coated side of the silicon wafer was connected to the conductive part of the substrate using an Ag/AgCl paste (Sigma-Aldrich, silver/silver chloride [60/40, 901773-50G]). The Ag/AgCl paste was then cured by heat treatment at 150°C for 30 min in a thermostatic oven (ESPEC, Desk-Top Hi-Temp Chamber, ST-110). Subsequently, all areas (except for the

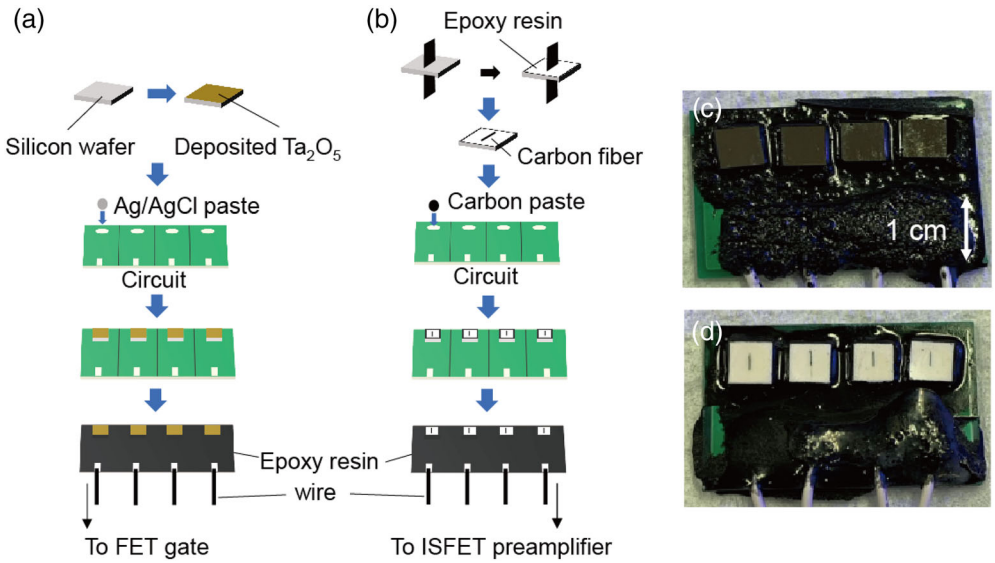

Fig. 1. Process used to fabricate the gate electrode and gate-voltage detection membrane. Steps involved in fabricating the (**A**) gate electrode and (**B**) gate-voltage detection membrane. Images of the (**C**) fabricated gate electrode and (**D**) gate-voltage detection membrane.

ion-sensitive areas) were insulated with epoxy resin (Sunhayato, Inpei Black) and mixed with resin and hardener (25 : 2 ratio). The FET was soldered onto a dedicated substrate for fixation, and its gate section was connected to a silicon wafer substrate using conductors through soldering. In the present study, we adopted an extended gate field-effect transistor (EGFET) structure, in which the sensor unit is separated from the FET, allowing for greater flexibility in sensor design. A carbon fiber (Sano Factory, USL Spread Carbon Tape HTS40) was used as the gate-voltage detection membrane (Kayanne et al. n.d.; Kim et al. 2023), secured with epoxy resin to expose only the carbon fiber area and then fastened to the conductive part of the substrate using carbon paste. This configuration enhances mechanical durability and ensures consistent gate-voltage detection while also providing improved stability and response characteristics due to the high conductivity and chemical resilience of carbon fiber.

Evaluating the multichannel ISFET-pH sensor array using standard solutions in a laboratory setting

The fabricated sensors were evaluated using standard pH solutions, Tris and AMP buffers in artificial seawater, and natural seawater to verify their stability and pH responses via gate-voltage measurements. The ISFET-pH sensors developed in this study were assessed by measuring the gate voltage while immersing them in three types of standard pH solutions (pH 9.18, 6.86, and 4.01; NBS scale), two types of artificial seawater (Tris and AMP; total scale), and natural seawater (total scale). The pH responses and sensitivities of the sensors were evaluated by immersing them in both a pH standard solution and Tris and AMP buffers in artificial seawater for approximately 10 min. pH sensitivity, defined as the change in gate voltage per unit pH (mV/pH), was assessed by immersing the sensors in pH standard solutions and Tris and AMP buffers in artificial seawater. The sensory stabilities were assessed by immersing them in natural seawater for approximately 1 d. All experiments were conducted at room temperature (25°C). Figure 2A shows the pH measurement system, which consists of an ISFET-pH sensor, gate-voltage detection membrane comprising carbon fiber, ISFET preamplifier, data logger (provided by Mobius Advanced Technology), and battery (IMPULSE AA rechargeable battery, Toshiba Electronic Devices & Storage). Before conducting the main experiments, a preliminary experiment was performed to determine the optimal drain current (I_d) for each sensor. This experiment was conducted at temperature conditions of 25°C and 40°C using a thermostatic chamber (ST-110, ESPEC Corp.). The gate-source voltage and I_d were measured in a pH 6.86 solution, and the drain-source voltage was set to 1.5 V. The intersection points of the characteristic curves at each temperature were identified. These intersection points were set as the optimal I_d for each sensor to minimize the effects of temperature fluctuations. Consequently, each sensor had a different target drain current, ranging from 486 to 623 μA.

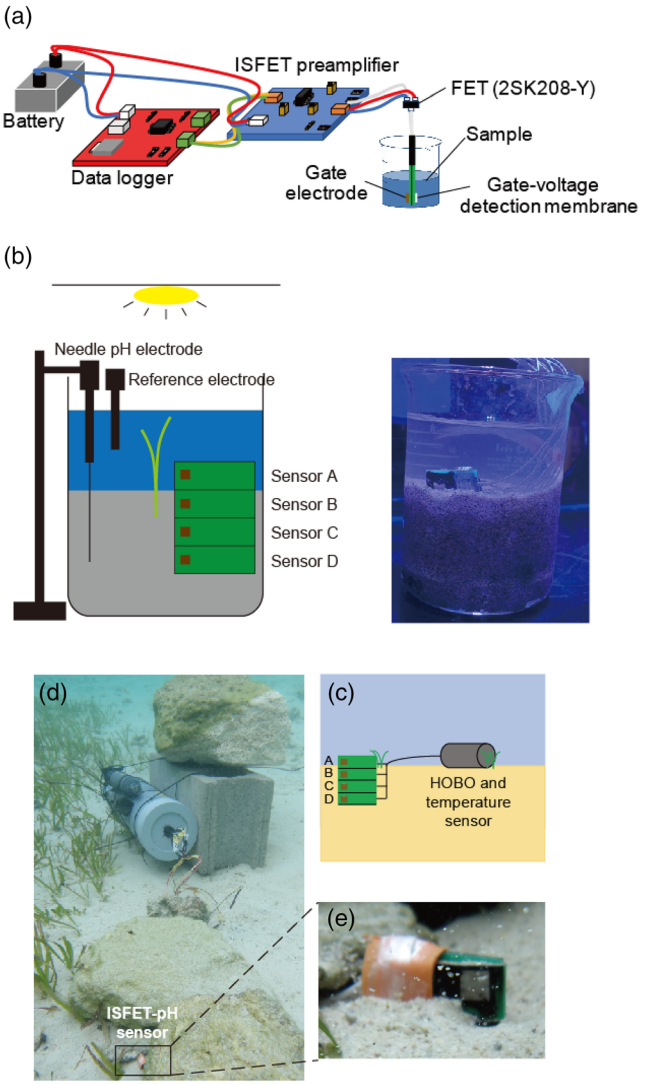

Fig. 2. Schematic representation and photograph of each experiment. (**A**) pH measurement system using ion-sensitive field-effect transistor (ISFET)-pH sensors, (**B**) schematic illustration (left) and photograph (right) of the simulated marine environment setup used in this study. The setup includes a needle pH electrode, a reference electrode, and four ISFET-pH sensors. (**C**–**E**) Deployment of the multichannel ISFET-pH sensor array. (**C**) Schematic representation of the pH distribution measurements obtained using the multichannel ISFET-pH sensor array. (**D**) Actual photograph of the sensor setup in a marine environment. (**E**) Close-up view of the ISFET-pH sensors embedded in marine sediments.

Evaluating the multichannel ISFET-pH sensor array in aquarium experiments

Figure 2B illustrates the simulated marine environment constructed in this study. Sand and seawater were collected from the main island of Okinawa, and the seagrass species *Thalassia hemprichii* was sourced from Churaumi Tropical Fish (https://chura-umi.com/). A single seagrass plant was placed in a 500-mL beaker, covered with approximately 10 cm of sand to bury its roots completely, and then filled with

approximately 400 mL of seawater. The light source, an AI Hydra 26D (D-D; The Aquarium Solution Ltd.), was set to simulate daylight conditions from 08:00 h to 18:00 h and was turned off for the rest of the day to reflect nighttime conditions. All experiments were conducted at a controlled temperature of 25°C.

We utilized a multichannel ISFET-pH sensor array comprising four fabricated ISFET-pH sensors. One sensor was placed in the water column, whereas the other three were positioned vertically in the sand. The distances from the sand surface were as follows: Sensor A at 3.5 mm (in the water column), Sensor B at − 3.5 mm, Sensor C at − 10.5 mm, and Sensor D at − 17.5 mm. This setup enabled us to measure the pH in the water column and vertical pH distribution in the sediment. The gate-voltage detection membrane was attached to the back of the gate electrode in a one-to-one manner. Needle-type glass pH electrodes (UPH-N) and the reference electrode, robust-type (UREF-RM), both manufactured by Unisense (Aarhus, Denmark), were used for comparative measurements.

The pH values in the simulated marine environment were measured continuously for 24 h. Using the needle-type pH electrode, vertical profiles were measured three times at 1-h intervals after starting the measurements and four more times until the measurements concluded the following day. Vertical pH profiles were obtained by vertically moving the needle-type pH electrode in the water column using a clamp and inserting it into the sand. The depths of the needle tips aligned with the positions of the multichannel ISFET-pH sensors, and measurements were recorded for 1 min at each depth. Additionally, outside the time for the vertical-profile measurements, the needle electrode measured the pH of the water column for comparison with Sensor A. Both the multichannel ISFET-pH sensors and needle-type pH sensors were calibrated before and after the measurements using Tris and AMP solutions for approximately 10 min each.

Evaluating the multichannel ISFET-pH sensor array through field observations

Our multichannel ISFET-pH sensor array was deployed in the shallow waters off Bise Beach, Motobu Town, Okinawa, Japan (26°42′30.1″N, 127°52′46.5″E) to measure pH distributions from October 8–10, 2023. One sensor was placed in the water column, and the other three were placed vertically on the sandy substrate. This setup enabled measurements of the water column pH and the vertical pH distribution within the sediments, with measurements recorded every second. The sensors were spaced 7.5 mm apart, enabling observations at depths of 2.5, 10.0, and 17.5 mm within the sediment. Figure 2C–E show a schematic and photographs of the pH distribution measurement system. Gate-voltage detection membranes were attached to the back of each gate electrode to ensure one-to-one correspondence. The multichannel ISFET-pH sensor array was secured in the sediment by putting a weight on the wires and was calibrated using Tris and AMP buffers on the total scale after the measurements. Additionally, a glass pH electrode (HOBO, MX2501) was used for comparative measurements. It was also calibrated using Tris and AMP buffers on the total scale after the measurements and pH recorded every 15 min. Temperature and salinity were continuously monitored using a compact memory temperature and salinity meter (JFE Advantech, DEFI2-CT), with data recorded every 15 min. To account for temperature variations in the field, a temperature compensation procedure was applied to the ISFET-pH sensor readings. The Nernst equation describes the theoretical temperature dependence of the sensor response:

$$S(T) = S(T_{\mathrm{calib}}) \times \frac{T}{T_{\mathrm{calib}}}$$

where $S(T)$ is the sensor sensitivity (mV/pH) at field temperature T, and $S(T_{\mathrm{calib}})$ is the sensitivity at the calibration temperature T_{calib}. The temperature-compensated pH value was calculated using:

$$\mathrm{pH}(T) = \mathrm{pH}_{\mathrm{Tris}} + \frac{E(T) - E_{\mathrm{Tris}}}{S(T)}$$

where $\mathrm{pH}_{\mathrm{Tris}}$ is the pH of the Tris buffer at calibration temperature T_{calib}, $E(T)$ and E_{Tris} are the ISFET sensor voltages at the field and calibration temperatures, respectively. This correction ensures consistency in pH measurements despite temperature fluctuations. Unisense needle-type electrodes were originally planned for vertical profile measurements; however, data collection was unsuccessful due to equipment malfunction.

Assessment

Evaluation of the tantalum oxide film

The thicknesses of tantalum oxide films deposited by sputtering were measured using an atomic force microscope. Half of a silicon wafer was masked to measure the film thickness, and the height difference at the boundary between the coated and uncoated areas was determined. The estimated film thickness was approximately 32 nm.

Furthermore, photoelectron spectra were obtained to focus on Ta and O within the deposited tantalum oxide film and analyzed via XPS. The elemental ratio on the surface of the film was determined based on the integrated peak areas of the measured spectra. The measured photoelectron spectra are shown in Fig. 3A. Elemental ratios were calculated by comparing the peak areas of the Ta 4f and O 1s orbitals. Notably, the Ta 4f orbital included the 4f 5/2 and 4f 7/2 orbitals; therefore, the peak area was halved for accurate elemental ratio calculations. The O : Ta ratio of the tantalum oxide film produced in this study was 3.16. This value is significantly higher than the theoretical O/Ta ratio of 2.5, showing approximately 26%

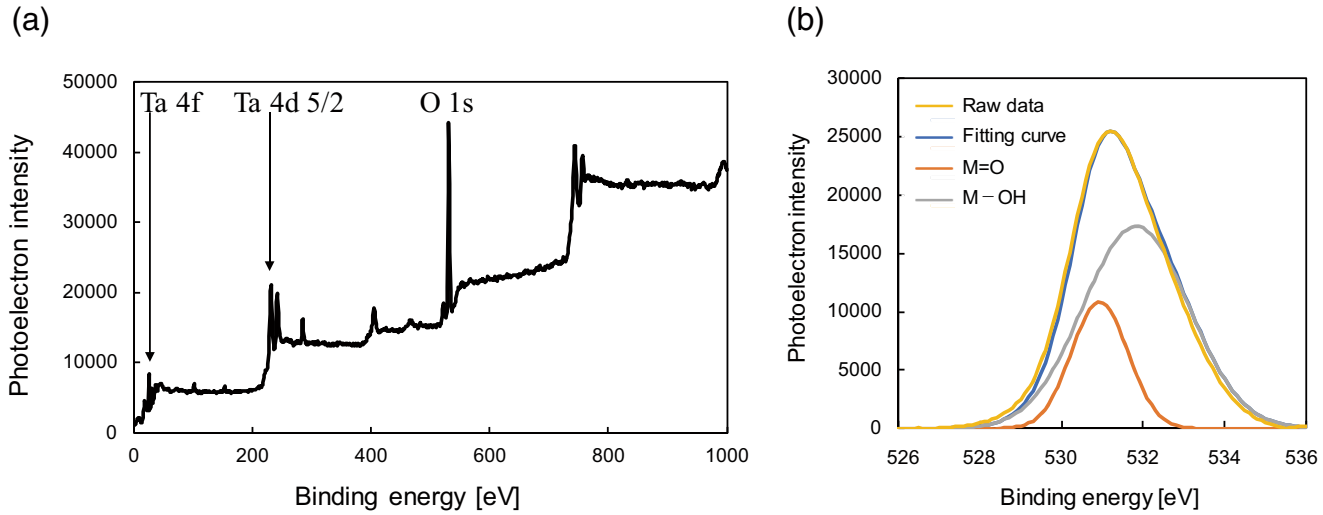

Fig. 3. Photoelectron spectrum of the deposited tantalum oxide film. (**A**) Complete data. (**B**) Peaks derived from O 1s and peaks after waveform separation.

deviation from the expected stoichiometry for the target material used in film deposition. We attributed this discrepancy to the ability of XPS to detect O even in a vacuum, leading to an overestimation of the O 1s peak. Subsequently, the peaks derived from O 1s were isolated and deconvoluted into peaks originating from the oxo and hydroxyl groups, enabling the determination of the respective ratios on the tantalum oxide surface. Figure 3B shows the deconvoluted and original O 1s peaks. The oxo and hydroxyl groups typically exhibited peaks at 529–530 eV and 531–532 eV, respectively (Amadine et al. 2017; Xu et al. 2021). Calculating the peak areas revealed that the hydroxyl : oxo group ratios were 561,976 and 187,550, respectively, resulting in a hydroxyl : oxo ratio of 3.00. These data suggest that the presence of hydroxyl groups on the surface enhances the film's interaction with H^+ ions, likely improving its pH sensitivity.

Evaluation of the pH responses of the fabricated multichannel ISFET-pH sensor array

We evaluated the ISFET-pH sensor developed in this study using three standard pH solutions (pH 9.18, 6.86, and 4.01), two types of artificial seawater (Tris and AMP), and natural seawater. pH sensitivity is defined as the change in gate voltage per unit pH (mV/pH). The evaluation involved measuring the gate voltage when the sensor was immersed in these solutions using a gate-voltage detection membrane made of carbon-fiber tape.

The responses of the sensor to the three pH standard solutions and the corresponding calibration curves are illustrated in Fig. 4A, B. The measurements indicated a sensitivity ranging from 38.7 to 53.8 mV/pH, with an estimated response time of 1–2 min. The theoretical Nernstian response at 25°C is ~ 59.16 mV/pH. In the present study, the sensitivity of the ISFET-pH sensors ranged from 38.7 to 53.8 mV/pH, corresponding to approximately 65–91% of the Nernstian response. This deviation from the theoretical value may be attributed to factors such as surface conditions of the sensor membranes, temperature influences, and individual differences in the FETs (Tintelott et al. 2021). A detailed discussion of these factors is provided in the Discussion section. The correlation coefficient (R^2) for each sensor was approximately 0.97–0.99, indicating high linearity. The resolution, determined using the 3σ method (Uemoto 2010), ranged from 0.0052 to 0.0093 pH. Noise was observed when transferring the sensor between standard solutions with different pH levels, which was attributed to the lack of a complete circuit between the gate electrode and gate-voltage detection membrane when not immersed in solution, preventing feedback control.

The sensor responses to Tris and AMP buffers in artificial seawater and the generated calibration curves are depicted in Fig. 4C, D. The measurements showed a sensitivity range from 26.0 to 59.1 mV/pH, with a response time of 1–2 min. The theoretical Nernstian response at 25°C is ~59.16 mV/pH. In the present study, the sensitivity of the ISFET-pH sensors in Tris and AMP buffers in artificial seawater ranged from 26.0 to 59.1 mV/pH, corresponding to approximately 44–99% of the Nernstian response. This deviation may be attributed to factors such as surface conditions of the sensor membranes, temperature influences, and individual differences in the FETs, which will be discussed in more detail in the Discussion section. The resolution, calculated using the 3σ method (Uemoto 2010), was in the 0.0021–0.033 pH range. For natural seawater measurements, pH conversion was performed using a calibration curve based on Tris and AMP buffers in artificial seawater gate-voltage measurements.

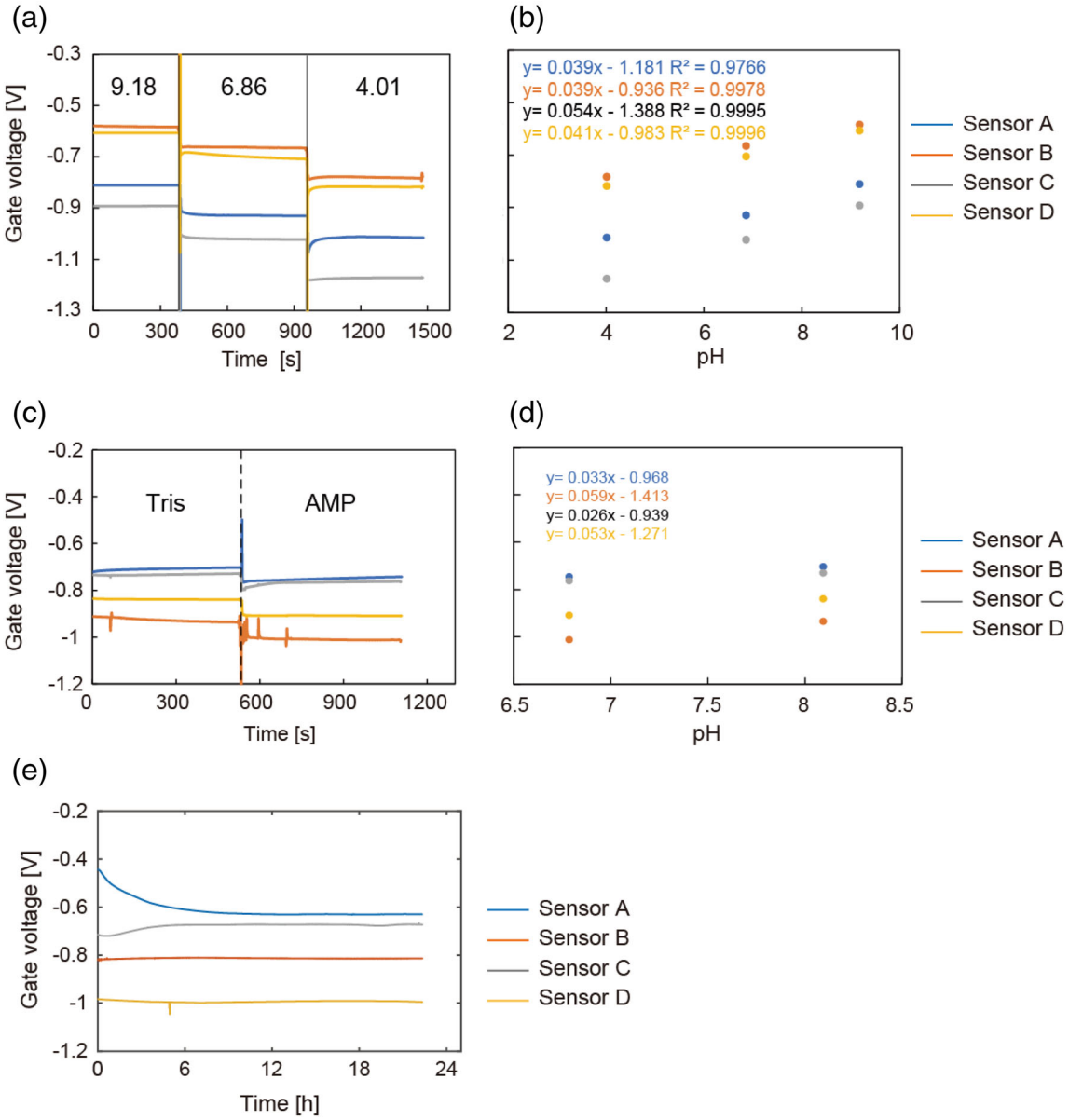

Fig. 4. Relationship between gate voltage and standard pH solutions. (**A**) Gate-voltage responses to different standard pH solutions (pH values: 9.18, 6.86, and 4.01). (**B**) Calibration curves derived from the gate-voltage measurements. (**C**) Gate-voltage responses to artificial seawater with Tris and AMP. (**D**) Calibration curves derived from the gate-voltage measurements in Tris and AMP buffers in artificial seawater. (**E**) Temporal gate-voltage variations when immersed in natural seawater.

Finally, to evaluate the stability of the fabricated ISFET-pH sensors, they were immersed in natural seawater for approximately 1 day. Figure 4E illustrates the variation in gate voltage measured in natural seawater. To quantify stability, the drift from the response time to the measurement endpoint was converted to pH on the total scale using the calibration curve. The estimated drift corresponded to 0.0054–0.028 pH over 12 h. The response time, defined as the duration until $100 \times |X - X_t|/|X|$ fell below 0.1%, was calculated. Here, X is the average gate voltage 1 h after measurement completion, and X_t is the gate voltage t after the measurement starts. The gate voltage stabilized after 9.7–12.5 h. After a conditioning period of approximately half a day, the ISFET-pH sensors exhibited stable gate voltages in natural seawater. However, further improvements to reduce drift are necessary for long-term field deployments.

Evaluation of the fabricated multichannel ISFET-pH sensor array in aquarium experiments

Figure 5A shows the temporal change in pH measured using the multichannel ISFET-pH and needle-type pH sensors. In the ISFET sensor array, all sensors exhibited instability and

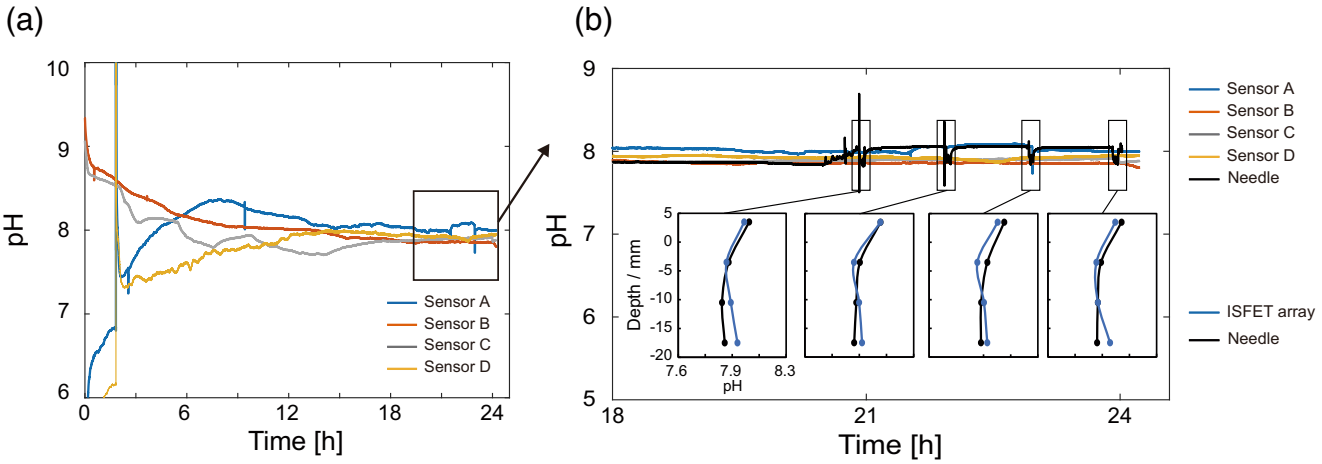

Fig. 5. Temporal pH changes in an aquarium experiment. (**A**) Measurements of 24-h pH variations with ISFET sensors. (**B**) Detailed pH fluctuations and vertical profiles during the 18–24-h period, as measured by ISFET sensors and a needle pH sensor.

drift during the first 12 h, which could be attributed to insufficient acclimation to seawater. Therefore, pH conversion was performed based on the calibration results. When examining more stable periods, the pH measured in the water column by Sensor A was approximately 0.1 units higher than that in the sediment. This finding suggests that sediment represents a relatively closed environment with limited seawater circulation, resulting in higher CO_2 concentrations due to respiration by microorganisms and *T. hemprichii* roots than in the water column.

Figure 5B shows the time-series changes and vertical pH distribution profiles of both sensors during the 18–24-h period. The pH of the needle-type pH sensor was measured for 60 s at each depth, and the average value for the last 30 s before moving to the next depth was plotted. The pH values measured by the needle-type pH sensor also showed that the pH in the water column was approximately 0.1–0.3 units higher than that in the sediment, consistent with the results from the ISFET sensor array. Moreover, the pH measurements from the fabricated multichannel ISFET-pH sensor array and the needle-type pH electrode matched well within a range of ± 0.05 for all profiles. Additionally, during intervals when the vertical profiles were not measured, the needle-type pH sensor monitored depths similar to Sensor C during the first half (18–20.5 h) and the water column, similar to Sensor A, during the second half (21–24 h). Even at these intervals, the measurements obtained using both methods were highly consistent. These results suggest that our multichannel ISFET-pH sensor array demonstrated sufficient reliability in controlled aquarium experiments.

Evaluation of the fabricated multichannel ISFET-pH sensor array through field observations

Field deployment and data collection

We measured pH distributions in marine sediments for approximately 2 d in the shallow waters off Bise Beach, Motobu Town, Okinawa, Japan, at a depth of approximately 1 m. The weather remained mostly clear during the observation period. The water temperature ranged from 27.5°C to 28.0°C, and the salinity was 34.3–34.4, except during low tide. During low tide, isolated tide pools formed, causing the water temperature to rise to 33°C and the salinity to drop to 31. The temporal pH changes (calibrated with Tris and AMP buffers) are shown in Fig. 6A. All pH values were reported on the total scale. The sensor array was configured as follows: Sensor A was placed in the water column, Sensor B in the first layer of marine sediments (depth: 2.5 mm), Sensor C in the second layer (depth: 10.0 mm), and Sensor D in the third layer (depth: 17.5 mm). Field observations began at 13:00 h on October 8, 2023, and approximately 48 h of data were collected at 1-s intervals. The daytime period from 06:30 to 18:00 h is indicated in yellow, whereas the nighttime period from 18:00 to 06:30 h is indicated in blue. The pH measurements exhibited instability during the initial 24 h, likely due to the conditioning requirements of ISFET sensors in natural seawater. This phenomenon has been reported in previous studies by Johnson et al. (2016) and Saba et al. (2019). In our study, all sensors, excluding Sensor B, were pre-soaked in seawater on October 7, the day before the field observations. The results suggest that approximately 2 d were required for the electrode surfaces to stabilize in field seawater, whereas stabilization occurred within 1 d under laboratory conditions. The extended stabilization time in the field may be attributed to interactions with various ions and organic matter in seawater. Although some sensors exhibited slight noise even after the initial 24 h, the measurements generally stabilized, yielding consistent observations.

Sensor performance and vertical profile

Figure 6B illustrates the pH time series for each sensor and the representative vertical pH profiles on day 2 (October 9–10, 2023). Each profile represents the average daytime and

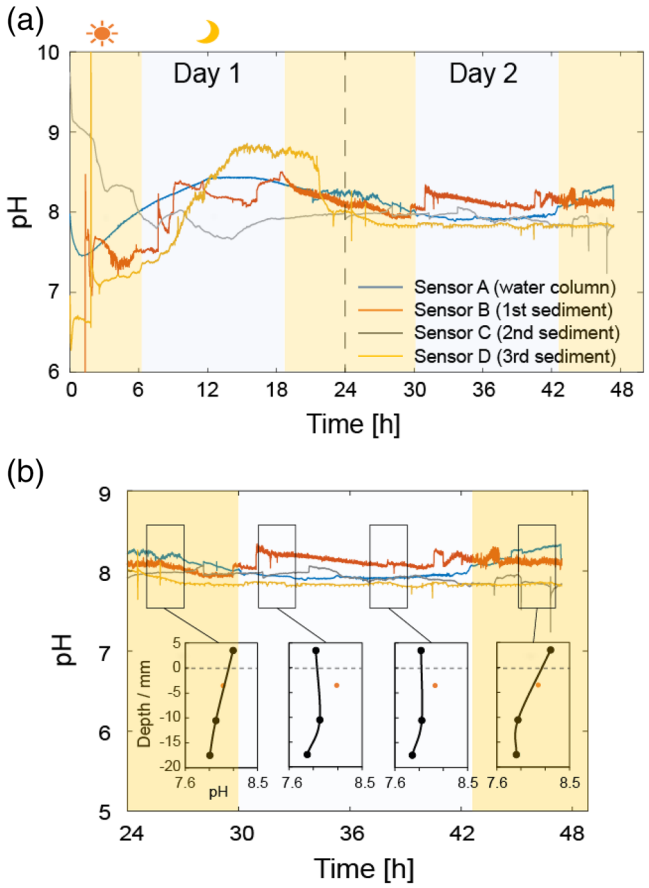

Fig. 6. (**A**) Temporal pH changes in marine sediments and the water column over 2 d at Bise Beach, Okinawa, Japan. The pH was measured using four sensors: Sensor A (water column, blue line), Sensor B (1st sediment layer at a depth of 2.5 mm, orange line), Sensor C (2nd sediment layer at a depth of 10 mm, gray line), and Sensor D (3rd sediment layer at a depth of 17.5 mm, yellow line). (**B**) Temporal pH changes and depth profiles in marine sediments and the water column on day 2 (October 9–10, 2023). The four profiles shown represent the average values plotted for the following periods: October 9, 14:00–16:00 h; October 9, 20:00–22:00 h; October 10, 02:00–04:00 h; and October 10, 10:00–12:00 h.

nighttime values derived from data collected at the following time intervals: 14:00–16:00 h and 20:00–22:00 h on October 9, 2023, and 02:00–04:00 h and 10:00–12:00 h on October 10, 2023. Sensor B, positioned near the sediment–seawater interface, experienced greater environmental fluctuations, leading to increased noise levels and measurement instability. Additionally, inadequate pre-soaking in seawater may have contributed to measurement inaccuracy. Consequently, data from Sensor B were excluded from further analysis.

The pH dynamics of the water column and sediment were then examined. In the water column, pH increased to 8.2–8.3 during the daytime and decreased to approximately 7.9 at night. The study site at Bise Beach is characterized by a high density of *T. hemprichii* (Higuchi et al. 2014). Photosynthetic activity by seagrasses, such as *T. hemprichii*, during daylight hours increased pH, whereas respiration at night led to pH reduction. The processes contributed to the observed diurnal variation. Similar trends were observed in the sediments, where pH fluctuated within a narrower range of 7.8–7.9. The reduced variability in sediment pH was likely due to limited seawater exchange compared to that in the water column. The trends are consistent with findings from previous studies (Rao et al. 2012; Yamamoto et al. 2015) and validate the effectiveness of our developed sensor system.

Comparison with commercial glass electrodes

We compared the pH values measured with ISFET-pH sensors with those obtained from a commercial glass pH electrode (HOBO MX2501) deployed in the water column. Figure 7A shows the temporal pH changes measured using Sensor A and HOBO glass electrode on October 9–10, 2023. Both sensors were positioned at approximately the same depth in the water column. The pH trends measured by the ISFET-pH sensor and the HOBO electrode were highly correlated. To quantify the agreement between the two sensors, we calculated the mean absolute error (MAE) as follows:

$$\mathrm{MAE} = \frac{1}{n}\sum_{k=1}^{n}\sqrt{\left(\mathrm{pH_{HOBO}} - \mathrm{pH_{EG-ISFET}}\right)^2} = 0.044$$

where n represents the number of data points. This small MAE indicates a high level of agreement between the two methods. This value indicates that the pH measurements from both sensors were highly comparable. The results suggest that the ISFET-pH sensors developed in this study observed pH distributions continuously within marine sediments.

We conducted Bland–Altman plot analysis as a further comparison. Figure 7B shows a comparison between the pH measurements obtained using the ISFET-pH sensor and the HOBO glass pH electrode. The central black line indicates the mean difference between both measurement methods. The mean pH difference was approximately 0.02. A mean difference close to zero suggests minimal systematic bias between the two methods. The observed bias was within the acceptable range, considering that the precision of the HOBO sensor is specified as ± 0.1 pH. The upper and lower dotted lines represent the limits of agreement, calculated as the mean difference ± 1.96 times the standard deviation of the differences, assuming a normal distribution of measurement differences. Most data points (over 97%) fell within the agreement limits (± 0.07 pH), suggesting that the measurements with both methods were generally consistent. The ISFET-pH sensor developed in this study demonstrated a measurement precision of ± 0.07 pH, as determined by the limits of agreement in the Bland–Altman analysis. The mean difference between the ISFET and HOBO sensors was approximately 0.02 pH, indicating minimal systematic bias. Given that the precision of the HOBO MX2501 sensor is specified as ± 0.1 pH, the ISFET-pH sensor exhibited comparable or superior precision.

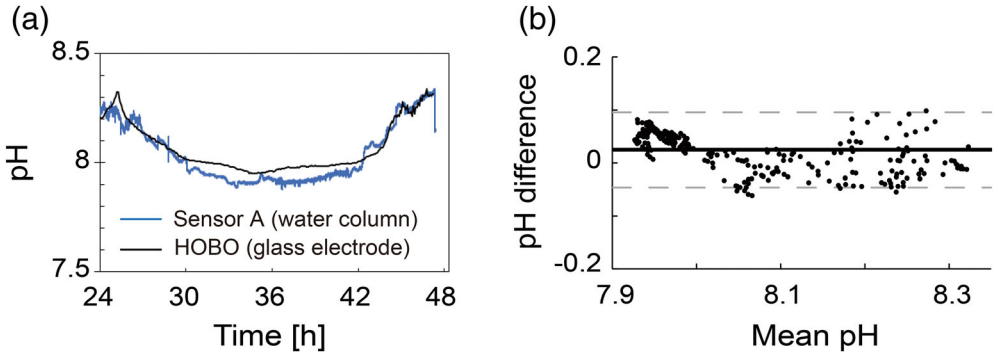

Fig. 7. Comparison of pH measurements between the HOBO glass pH electrode and the ISFET-pH sensor. (**A**) Time-series pH measurements over 24 h in the water column, showing the data from Sensor A (blue line) and the HOBO glass electrode (black line). (**B**) Bland–Altman plot comparing the pH measurements obtained with the ISFET-pH sensor and the HOBO glass electrode, illustrating the mean pH difference and the limits of agreement. The *x*-axis represents the average pH values (mean pH) measured by both sensors, whereas the *y*-axis shows differences in the pH values found with the two methods.

Discussion

Features of our developed sensor and comparison with existing products

Table 1 compares the multichannel ISFET-pH sensor array developed in the present study with a needle-type glass pH electrode (Unisense). The ISFET-pH sensor demonstrated several advantages over conventional glass electrodes, particularly in terms of cost, durability, and continuous monitoring capabilities. The sensor was moderately priced at less than $50 per unit and was highly robust, making it less prone to breakage. In contrast, the needle-type glass pH electrode alone was significantly more expensive, costing approximately $2500, and it was fragile.

Both sensors exhibited a precision of less than 0.1 pH. However, the ISFET-pH sensor allowed for continuous monitoring with automatic operation, requiring minimal manual intervention. In contrast, the needle-type glass electrode was limited to snapshot measurements, as it required manual operation, which was labor intensive and time consuming.

The ISFET-pH sensor was designed for embedded use, minimizing disturbance to the sediment environment and enabling real-time data collection without delays. In contrast, the needle-type glass electrode had to be inserted manually, which could disrupt the profile environment and introduce time lags in data acquisition. The characteristics highlight the advantages of the ISFET-pH sensor for continuous in situ measurements, making it a promising alternative to conventional needle-type pH electrodes.

Table 1. Comparison of pH values obtained with a multichannel ISFET sensor and a needle pH sensor.

Criteria	Multichannel ISFET sensor	Needle pH sensor
Price	Moderate (< $50)	High (~ $2500)
Durability	Robust, less prone to breakage	Fragile, prone to breakage
Measurement precision	High (< 0.1)	High (< 0.1)
Time continuity	Capable of continuous monitoring	Snapshot
Operation	Automatic, minimal manual intervention	Manual; requires labor operation
Impact on environment	Does not alter the profile environment	Intrusive; may alter profile environment
Profile measurement time	Real-time data collection with no lag	Time lag attributed to manual operation

Nernst response deviation

The ISFET-pH sensors developed in the present study exhibited a sensitivity ranging from 26.0 to 59.1 mV/pH, which deviated from the theoretical Nernstian response (59.16 mV/pH). According to table 2 in Sinha and Pal (2022), many studies on EGFET-based pH sensors have reported deviations from the Nernstian response, and our results are consistent with these findings. The possible causes of this deviation are as follows:

1. Structural factors and surface conditions of the ISFET gate electrode: The presence of oxygen vacancies formed during film deposition may not have been uniform among the sensors. Variations in the distribution of oxygen vacancies can restrict proton response and cause fluctuations in pH sensitivity.
2. Limitation of proton response due to adsorbed ions: Accumulation of adsorbed ions such as Na^+ and Cl^- on the tantalum oxide surface may have suppressed proton response, leading to a reduction in sensitivity.
3. Screening effect of the compressed double layer: In high ionic strength solutions, the electrical double layer becomes

compressed, reducing the extent to which H^+ potential changes are transmitted to the sensor. This phenomenon is one possible reason why the sensitivity was lower than the theoretical Nernstian response.

4. Variations among individual FET devices: Small manufacturing variations among FET devices could have contributed to differences in sensor sensitivity.

The factors above likely acted jointly, resulting in the observed deviation from the theoretical Nernstian response. To minimize the variability in sensor sensitivity, we performed post-calibration and converted pH values based on calibration curves. This compensation improved measurement precision; however, further improvements are necessary. In particular, optimizing sputtering conditions and annealing processes could enhance the uniformity of tantalum oxide films.

Challenges and potential applications

Although the multichannel ISFET-pH sensor array developed in the present study offers significant advantages over conventional needle-type glass electrodes, several challenges remain that must be addressed to improve its performance and applicability. One of the primary issues is the susceptibility to noise, particularly due to cable interference. In the present study, nonspecialized cables were used, which increased the likelihood of external electrical interference. Additionally, unprocessed 24-bit data were collected every second, which could introduce noise fluctuations. Future improvements should focus on optimizing data processing algorithms and utilizing shielded cables to enhance signal stability.

Another challenge is the sensor's stabilization time in seawater. The results indicated that approximately 12–24 h were required for the sensor response to stabilize after deployment. This was likely due to the insufficient pre-soaking of sensors before field observations. Pre-conditioning the sensors in seawater prior to deployment may enhance initial stability and reduce data inconsistencies among sensors.

Despite the challenges above, the developed sensor array demonstrates strong potential for various applications. One of its key advantages is its ability to be embedded within sediments, allowing for continuous in situ pH monitoring without disturbance of the surrounding environment. This feature makes it particularly useful for studying sediment biogeochemistry, carbonate dissolution, and microbial activity, which require fine-scale temporal and spatial pH measurements.

Additionally, the ability to capture high-resolution pH profiles at millimeter-scale intervals provides valuable insights into chemical processes occurring at the sediment–water interface. Refinements in sensor configuration, such as increasing the density of sensor elements or utilizing thin-film sensor technologies, such as PET-based layers, could further improve the vertical resolution of pH profiles. Such advancements would enhance the sensor's capability to quantify carbonate dissolution fluxes and other critical geochemical processes in marine sediments.

However, unlike our experimental conditions (undisturbed sandy sediments), heterogeneous or high-energy environments present several challenges, including sensor instability, disturbance of the sediment structure, and potential interference from suspended particles. These limitations can be minimized by developing protective housings for the sensor, improving anchoring methods, using contamination-resistant coatings, and implementing real-time position monitoring technologies to enable stable, accurate, and long-term measurements under diverse environmental conditions.

Beyond coral reef environments, this sensor system could be adapted for other aquatic applications, such as monitoring pH variations in estuaries, lakes, and riverine sediments. Further refinements in sensor technology and deployment methods will enhance its applicability in diverse aquatic ecosystems. However, the precision of approximately $\pm$ 0.07 pH does not meet the climate-quality data requirement of $\pm$ 0.003 pH set by the Global Ocean Acidification Observing Network. Therefore, this sensor is not yet suitable for open-ocean climate monitoring or long-term applications requiring high precision. Notwithstanding, this sensor can be used in weather-quality data collection ($\pm$ 0.02 pH) and in investigating biogeochemical dynamics in sediment pore water, where continuous fine-scale measurements are critical.

Comments and recommendations

In the present study, we proposed a novel approach for continuously measuring pH distribution in sandy sediments by embedding an array of ISFET sensors directly into the sediment. Unlike conventional methods that rely on inserting glass electrodes, this technique enables real-time monitoring of fine-scale pH variations within the sediment, which was previously difficult to achieve. This approach has the potential to serve as a powerful tool for quantitatively evaluating the chemical role of sandy sediments and elucidating their contributions to carbon cycling and pH fluctuations in coral reef ecosystems.

However, challenges remain regarding the measurement precision of the developed sensor. As demonstrated by the Bland–Altman analysis, the precision of this sensor was approximately $\pm$ 0.07 pH, which is comparable to that of commercially available glass electrodes ($\pm$ 0.1 pH) but does not match the higher precision of spectrophotometric pH measurements ($\pm$ 0.005 pH) and commercial ISFET-based sensors such as DuraFET ($\pm$ 0.01–0.02 pH). Future studies should include direct comparisons between the ISFET-pH sensor and spectrophotometric pH measurements using purified meta-cresol purple indicators to assess the accuracy of the sensor in marine environments. This would provide a more comprehensive evaluation of its suitability for carbonate chemistry monitoring. To improve precision, further optimization of sputtering conditions and annealing processes is required to enhance the uniformity of the tantalum

oxide membrane. Additionally, incorporating data correction techniques to mitigate environmental influences on measurements will be essential.

The ISFET-pH sensor developed in the present study is specialized for pH measurement and cannot directly measure other carbonate system parameters, such as alkalinity or total dissolved inorganic carbon. Since pH measurement alone is insufficient for comprehensive assessments of carbon cycling in marine environments, the development of sensors capable of simultaneously measuring additional carbonate system parameters is necessary. For example, modifying the sensing membrane to selectively detect alkalinity or carbonate ion concentrations could significantly expand the applicability of this approach to a broader range of marine studies. Given the increasing importance of long-term carbonate chemistry monitoring in response to ocean acidification, advancements in these sensor technologies will have major research significance.

Author Contributions

Yoshita Ogawa conducted the experiments, performed field investigations, processed the data, and wrote the manuscript. Shoji Yamamoto conceived the study, conducted the experiments, performed the field investigations, processed the data, and contributed to writing the manuscript. Kenta Suzuki and Kazuhiro Morioka conducted the experiments and critically revised the manuscript. Akihide Hemmi conceived the idea, conducted the experiments, and critically revised the manuscript. Hajime Kayanne and Hizuru Nakajima critically revised the manuscript, secured the funding, and managed the project.

Acknowledgments

This work was supported by the Japan Society for the Promotion of Science (JSPS) (KAKENHI; grant numbers 21H03578, 23K17464, and 24H01521). We thank Professor M. Yang and Professor A. Kaneko at Tokyo Metropolitan University for allowing us to use their equipment. We also thank all laboratory members and staff at Tokyo Metropolitan University, the University of Tokyo, and the University of the Ryukyus for their assistance and support.

Conflicts of Interest

The authors declare no conflicts of interest.

References

Amadine, O., Y. Essamlali, A. Fihri, M. Larzek, and M. Zahouily. 2017. "Effect of Calcination Temperature on the Structure and Catalytic Performance of Copper–Ceria Mixed Oxide Catalysts in Phenol Hydroxylation." *RSC Advances* 7: 12586–12597. https://doi.org/10.1039/C7RA00734E.

Andersson, A., J. Kuffner, I. B. Mackenzie, et al. 2009. "Net Loss of $CaCO_3$ from a Subtropical Calcifying Community Due to Seawater Acidification: Mesocosm-Scale Experimental Evidence." *Biogeosciences* 6: 1811–1823. https://doi.org/10.5194/bg-6-1811-2009.

Andersson, A. J., and D. Gledhill. 2013. "Ocean Acidification and Coral Reefs: Effects on Breakdown, Dissolution, and Net Ecosystem Calcification." *Annual Review of Marine Science* 5: 321–348. https://doi.org/10.1146/annurev-marine-121211-172241.

Bergveld, P. 1970. "Development of an Ion-Sensitive Solid-State Device for Neurophysiological Measurements." *IEEE Transactions on Biomedical Engineering* 17: 70–71. https://doi.org/10.1109/tbme.1970.4502688.

Bergveld, P. 2003. "Thirty Years of ISFETOLOGY What Happened in the Past 30 Years and What May Happen in the Next 30 Years." *Sensors and Actuators B: Chemical* 88, no. 1: 1–20. https://doi.org/10.1016/S0925-4005(02)00301-5.

Bresnahan, P. J., Jr., T. R. Martz, Y. Takeshita, K. S. Johnson, and M. LaShomb. 2014. "Best Practices for Autonomous Measurement of Seawater pH with the Honeywell Durafet." *Methods in Oceanography* 9: 44–60. https://doi.org/10.1016/j.mio.2014.08.003.

Dickson, A. G., C. L. Sabine, and J. R. Christian. 2007. Guide to Best Practices for Ocean CO_2 Measurements. North Pacific Marine Science Organization.

Doney, S. C., V. J. Fabry, R. A. Feely, and J. A. Kleypas. 2009. "Ocean Acidification: The Other CO_2 Problem." *Annual Review of Marine Science* 1: 169–192. https://doi.org/10.1146/annurev.marine.010908.163834.

Dove, S. G., D. I. Kline, O. Pantos, F. E. Angly, G. W. Tyson, and O. Hoegh-Guldberg. 2013. "Future Reef Decalcification under a Business-as-Usual CO_2 Emission Scenario." *Proceedings of the National Academy of Sciences* 110: 15342–15347. https://doi.org/10.1073/pnas.1302701110.

Eyre, B. D., A. J. Andersson, and T. Cyronak. 2014. "Benthic Coral Reef Calcium Carbonate Dissolution in an Acidifying Ocean." *Nature Climate Change* 4: 969–976. https://doi.org/10.1038/nclimate2380.

Eyre, B. D., T. Cyronak, P. Drupp, E. H. de Carlo, J. P. Sachs, and A. J. Andersson. 2018. "Coral Reefs Will Transition to Net Dissolving before End of Century." *Science* 359: 908–911. https://doi.org/10.1126/science.aao1118.

Gattuso, J. P., M. Frankignoulle, and R. Wollast. 1998. "Carbon and Carbonate Metabolism in Coastal Aquatic Ecosystems." *Annual Review of Ecology and Systematics* 2: 405–434. https://doi.org/10.1146/annurev.ecolsys.29.1.405.

Gonski, S. F., W. J. Cai, W. J. Ullman, et al. 2018. "Assessment of the Suitability of Durafet-Based Sensors for pH Measurement in Dynamic Estuarine Environments." *Estuarine, Coastal and Shelf Science* 200: 152–168. https://doi.org/10.1016/j.ecss.2017.10.020.

Gonski, S. F., G. W. Luther III, A. L. Kelley, et al. 2024. "A Half-Cell Reaction Approach for pH Calculation Using a Solid-State Chloride Ion-Selective Electrode with a Hydrogen Ion-Selective Ion-Sensitive Field Effect Transistor."

Marine Chemistry 261: 104373. https://doi.org/10.1016/j.marchem.2024.104373.

Higuchi, T., K. K. Takagi, K. Matoba, et al. 2014. "The Nutrient and Carbon Dynamics that Mutually Benefit Coral and Seagrass in Mixed Habitats under the Influence of Groundwater at Bise Coral Reef, Okinawa, Japan." *International Journal of Marine Science* 4: 1–15. https://doi.org/10.5376/ijms.2014.04.0001.

Jimenez-Jorquera, C., J. Orozco, and A. Baldi. 2010. "ISFET Based Microsensors for Environmental Monitoring." *Sensors (Basel)* 10: 61–83. https://doi.org/10.3390/s100100061.

Johnson, K. S., H. W. Jannasch, L. J. Coletti, et al. 2016. "Deep-Sea DuraFET: A Pressure Tolerant pH Sensor Designed for Global Sensor Networks." *Analytical Chemistry* 88: 3249–3256. https://doi.org/10.1021/acs.analchem.5b04653.

Kayanne, H., et al. n.d. "All-Solid-State Extended-Gate pH ISFET Sensor Developed Using Carbon-Based Gate Potential Applicator as an Alternative to Conventional Reference Electrodes." (Unpublished).

Kim, D. H., H. S. Cho, J. H. Kim, et al. 2023. "The Integration of Reference Electrode for ISFET Ion Sensors Using Fluorothiophenol-Treated rGO." *Biosensors* 13: 89. https://doi.org/10.3390/bios13010089.

Kroeker, K. J., R. L. Kordas, R. Crim, et al. 2013. "Impacts of Ocean Acidification on Marine Organisms: Quantifying Sensitivities and Interaction with Warming." *Global Change Biology* 19: 1884–1896. https://doi.org/10.1111/gcb.12179.

Martz, T. R., J. G. Connery, and K. S. Johnson. 2010. "Testing the Honeywell Durafet® for Seawater pH Applications." *Limnology and Oceanography: Methods* 8: 172–184. https://doi.org/10.4319/lom.2010.8.172.

McLaughlin, K., A. Dickson, S. B. Weisberg, et al. 2017. "An Evaluation of ISFET Sensors for Coastal pH Monitoring Applications." *Regional Studies in Marine Science* 12: 11–18. https://doi.org/10.1016/j.rsma.2017.02.008.

Miller, C. A., K. Pocock, W. Evans, and A. L. Kelley. 2018. "An Evaluation of the Performance of Sea-Bird Scientific's SeaFET™ Autonomous pH Sensor: Considerations for the Broader Oceanographic Community." *Ocean Science* 14, no. 4: 751–768. https://doi.org/10.5194/os-14-751-2018.

Müller, J. D., and G. Rehder. 2018. "Metrology of pH Measurements in Brackish Waters—Part 2: Experimental Characterization of Purified Meta-Cresol Purple for Spectrophotometric pHT Measurements." *Frontiers in Marine Science* 5: 177. https://doi.org/10.3389/fmars.2018.00177.

Newton, J. A., R. A. Feely, E. B. Jewett, P. Williamson, and J. Mathis. 2015. Global Ocean Acidification Observing Network: Requirements and Governance Plan. Second ed. GOA-ON. http://www.goa-on.org/docs/GOA-ON_plan_print.pdf.

Orr, J. C., V. J. Fabry, O. Aumont, et al. 2005. "Anthropogenic Ocean Acidification Over the Twenty-First Century and its Impact on Calcifying Organisms." *Nature* 437: 681–686. https://doi.org/10.1038/nature04095.

Rao, A. M. F., L. Polerecky, D. Ionescu, F. J. R. Meysman, and D. De Beer. 2012. "The Influence of Pore-Water Advection, Benthic Photosynthesis, and Respiration on Calcium Carbonate Dynamics in Reef Sands." *Limnology and Oceanography* 57: 809–825. https://doi.org/10.4319/lo.2012.57.3.0809.

Saba, G. K., E. Wright-Fairbanks, B. Chen, et al. 2019. "The Development and Validation of a Profiling Glider Deep ISFET-Based pH Sensor for High Resolution Observations of Coastal and Ocean Acidification." *Frontiers in Marine Science* 6: 664. https://doi.org/10.3389/fmars.2019.00664.

Shao, C., D. Tang, L. Legendre, Y. Sui, and H. Wang. 2023. "Vertical Distribution of pH in the Top ~10 m of Deep-Ocean Sediments: Analysis of a Unique Dataset." *Frontiers in Marine Science* 10: 1126704. https://doi.org/10.3389/fmars.2023.1126704.

Silverman, J., B. Lazar, L. Cao, K. Caldeira, and J. Erez. 2009. "Coral Reefs May Start Dissolving When Atmospheric CO_2 Doubles." *Geophysical Research Letters* 36: 2008GL036282. https://doi.org/10.1029/2008GL036282.

Sinha, S., and T. Pal. 2022. "A Comprehensive Review of FET-Based pH Sensors: Materials, Fabrication Technologies, and Modeling." *Electrochemical Science Advances* 2: e2100147. https://doi.org/10.1002/elsa.202100147.

Soetaert, K., A. F. Hofmann, J. J. Middelburg, F. J. R. Meysman, and J. Greenwood. 2007. "The Effect of Biogeochemical Processes on pH." *Marine Chemistry* 105: 30–51. https://doi.org/10.1016/j.marchem.2006.12.012.

Tintelott, M., V. Pachauri, S. Ingebrandt, and X. T. Vu. 2021. "Process Variability in Top-Down Fabrication of Silicon Nanowire-Based Biosensor Arrays." *Sensors* 21: 5153. https://doi.org/10.3390/s21155153.

Tribollet, A., C. Godinot, M. Atkinson, and C. Langdon. 2009. "Effects of Elevated pCO_2 on Dissolution of Coral Carbonates by Microbial Euendoliths." *Global Biogeochemical Cycles* 23: 2008GB003286. https://doi.org/10.1029/2008GB003286.

Uemoto, M. 2010. "Fundamental Knowledge for Reliable Analysis – Concepts and Definitions of the Limit of Detection and the Limit of Quantitation." *Bunseki* 5: 216–221.

Widdicombe, S., S. L. Dashfield, C. L. McNeill, et al. 2009. "Effects of CO_2 Induced Seawater Acidification on Infaunal Diversity and Sediment Nutrient Fluxes." *Marine Ecology Progress Series* 379: 59–75. https://doi.org/10.3354/meps07894.

Xu, X., L. Liu, Y. Tong, et al. 2021. "Facile Cr^{3+}-Doping Strategy Dramatically Promoting Ru/CeO_2 for Low-Temperature CO_2 Methanation: Unraveling the Roles of Surface Oxygen Vacancies and Hydroxyl Groups." *ACS Catalysis* 11: 5762–5775. https://doi.org/10.1021/acscatal.0c05468.

Yamamoto, S., H. Kayanne, T. Tokoro, T. Kuwae, and A. Watanabe. 2015. "Total Alkalinity Flux in Coral Reefs Estimated from Eddy Covariance and Sediment Pore-Water Profiles: Total Alkalinity Flux in Coral Reefs." *Limnology and Oceanography* 60: 229–241. https://doi.org/10.1002/lno.10018.

Yanagawa, K., Y. Morono, D. De Beer, et al. 2013. "Metabolically Active Microbial Communities in Marine Sediment under High-CO_2 and Low-pH Extremes." *The ISME Journal* 7: 555–567. https://doi.org/10.1038/ismej.2012.124.

Submitted 13 March 2025
Revised 07 April 2025
Accepted 02 July 2025